Pathobiology of Aging & Age-related Diseases

COACTION PUBLISHING

RESEARCH PAPER

Investigation and identification of etiologies involved in the development of acquired hydronephrosis in aged laboratory mice with the use of high-frequency ultrasound imaging

Danielle A. Springer[1]*, Michele Allen[1], Victoria Hoffman[2], Lauren Brinster[2], Matthew F. Starost[2], Mark Bryant[2] and Michael Eckhaus[2]

[1]Murine Phenotyping Core, National Heart, Lung, and Blood Institute, National Institutes of Health, Bethesda, MD, USA; [2]Office of Research Services, Division of Veterinary Resources, National Institutes of Health, Bethesda, MD, USA

Laboratory mice develop naturally occurring lesions that affect biomedical research. Hydronephrosis is a recognized pathologic abnormality of the mouse kidney. Acquired hydronephrosis can affect any mouse, as it is caused by any naturally occurring disease that impairs free urine flow. Many etiologies leading to this condition are of particular significance to aging mice. Non-invasive ultrasound imaging detects renal pelvic dilation, renal enlargement, and parenchymal loss for pre-mortem identification of this condition. High-frequency ultrasound transducers produce high-resolution images of small structures, ideal for detecting organ pathology in mice. Using a 40 MHz linear array transducer, we obtained high-resolution images of a diversity of pathologic lesions occurring within the abdomen of seven geriatric mice with acquired hydronephrosis that enabled a determination of the underlying etiology. Etiologies diagnosed from the imaging results include pyelonephritis, neoplasia, urolithiasis, mouse urologic syndrome, and spontaneous hydronephrosis, and were confirmed at necropsy. A retrospective review of abdominal scans from an additional 149 aging mice shows that the most common etiologies associated with acquired hydronephrosis are mouse urologic syndrome and abdominal neoplasia. This report highlights the utility of high-frequency ultrasound for surveying research mice for age-related pathology, and is the first comprehensive report of multiple cases of acquired hydronephrosis in mice.

Keywords: *ultrasound*; *hydronephrosis*; *renal pelvic dilation*; *mice*; *abdominal imaging*; *kidney*; *pathology*; *mouse urologic syndrome*; *abdominal neoplasia*

*Correspondence to: Danielle A. Springer, National Institutes of Health, Building 14E, Room 105F, Service Road West, Bethesda, MD, USA 20893, Email: ds628k@nih.gov

Received: 14 May 2014; Accepted: 16 June 2014; Published: 1 August 2014

Acquired hydronephrosis develops when an obstruction impedes urine flow through the urinary tract, causing increased intrarenal pressure and expansion of the kidney with urine. One or both kidneys may be affected and the severity ranges from a dilation of the renal pelvis alone (mild hydronephrosis), to the progressive loss of the renal papilla, medulla, and cortex as the expanding urine filled pelvis compresses the parenchyma against the renal capsule (1–6). In severe cases, the enlarged kidney appears as a tense, round, fluid filled cyst surrounded by a thin border of remaining cortex (1,6–11).

Hydronephrosis is a recognized pathologic condition in the mouse, and can be congenital, hereditary, or acquired. Acquired hydronephrosis represents naturally occurring cases that arise during the lifetime of an animal after it acquires a condition that leads to an obstruction at any level of the urinary tract.

Causes of urinary tract obstructions in mice include: urolithiasis, pyelonephritis, prostate hypertrophy, bladder herniation; abdominal, pelvic and urinary system tumors or abscesses; urethral inflammation; fibrosis and scarring in the perineum from dermatitis or trauma; suppurative and hemorrhagic occlusions from cystitis; ascending urinary tract infections (UTI), seminal vesicle coagula, suppurative vesico-urethritis, renal papillary necrosis, and lesions to the smooth muscle cells and neurons of the peristaltic machinery (3,9,12–16). Acquired hydronephrosis can occur at any age but is more likely to afflict older

Citation: Pathobiology of Aging & Age-related Diseases 2014, **4**: 24932 - http://dx.doi.org/10.3402/pba.v4.24932

adult animals than congenital and hereditary hydronephrosis which tend to manifest in young mice.

While acquired cases occur sporadically in any strain, data detailing the incidences of strain, sex, and etiology have not been reported. Congenital and hereditary hydronephrosis in mice have been well documented. Strains with heritable hydronephrosis and reported incidences include: C57BL/KsJ (46% male) (11), NZC inbred mice (58% male, 81% female) (6), BRVR strains (40.5% male, 28% female) (5,8), DDD (100% male, 40% female) (2), KK-A^y (24/31 male) (9), STR/N (high incidence, age dependent) (10), and C57BL/6 (6% male, 9% female) (17). Hydronephrosis has been described for a number of well-known genetic mutations as well, including the luxate (18–20), luxoid (19–21), short ear (21), and dominant hemimelia (Dh) (19,20) mutations in the luxoid group of mutants, and the chronic progressive hydronephrosis (cph) (8,13), and the urogenital (11) mutations.

Hydronephrosis also occurs in transgenic (TG) and knockout (KO) mice with gene alterations affecting renal physiology, including Hspa 21 KO mice (22), p23 TG mice (23), NaK2CL co-transporter KO mice (4), and Aquaporin 2 KO mice (13). Mouse models with alterations regulating embryonic development of the renal collecting system have also been described, for example, *EphA4*$^{gf/gf}$ mice develop hydronephrosis associated with duplex collecting systems and ureters and impaired ureter peristalsis (24).

Genetically attributed hydronephrosis in mice clearly represents a diverse group encompassing numerous pathogenic mechanisms which lead to the development of a single abnormality. The luxoid gene mutations affect skeletal development with a reduction in vertebrae number and body cavity size (18–21). Hydronephrosis develops from kinks in the ureters as the reduced body cavity size cannot accommodate its length, from pressure imposed against the ureter from overcrowded organs, and abnormal ureteral vein terminations on the ureter (18,20,21). In contrast, loss of the NaK2CL co-transporter in NKCC2 KO mice (4) and a mutation in Aquaporin-2 in cph mice (13) both result in an inability to concentrate urine with severe polyuria and hydronephrosis in the absence of an obstruction. Models with alterations in the renin-angiotensin-aldosterone system develop a similar phenotype of polyuria, reduced urine osmolality, and hydronephrosis (25). Additional mouse models with hydronephrosis include: congenital hydronephrosis caused by ureteral strictures after exposure to 2, 3, 7, 8 – Tetrachlorodibenzo-p-dioxin (7,26); hydronephrosis caused by changes in urethral muscle tone after estradiol administration (1,27–29); and hydronephrosis from genetic alterations affecting non-renal systems as in the development of urinary tract strictures from auto-antibody deposition in mice deficient in various immune receptors (30).

Despite the large volume of literature describing hydronephrosis in mice, studies involving acquired hydronephrosis secondary to naturally occurring disease are scarce. Acquired hydronephrosis warrants special interest to researchers using mice in biomedical studies as the condition can occur during the lifetime of any mouse, causing alterations in kidney function and animal morbidity. Furthermore, many of the underlying etiologies are associated with age-related pathology. This report focuses on naturally occurring cases of acquired hydronephrosis detected in aged mice during abdominal ultrasound exams. Ultrasound imaging readily detected mice with hydronephrotic kidneys. Analysis of the ultrasound images also enabled a pre-mortem diagnosis of the primary disease process associated with the development of the hydronephrosis. A review of 156 abdominal scans in aging mice conducted within our facility provides information regarding the frequency and causes of this condition in multiple mouse strains. Ultrasound imaging enables the in vivo detection and diagnosis of clinical diseases affecting laboratory mice, and can lead to enhanced knowledge of natural age associated disease processes that impact research objectives and outcomes.

Methods

Animals and husbandry

Mice were housed in ventilated cage racks in an Association for Assessment and Accreditation of Laboratory Animal Care International (AAALAC) accredited animal facility at the National Institutes of Health (NIH), Bethesda, MD. Animal care, husbandry, and the housing environment were in accordance with the Guide for the Care and Use of Laboratory Animals (31). NIH Animal Care and Use Committees approved the animal protocols.

Abdominal ultrasound

Two-dimensional images of the kidneys and abdominal organs were acquired using the Vevo2100 ultrasound system (VisualSonics, Toronto, Canada) with a 40 MHz ultrasound probe (MS550D, VisualSonics, Toronto Canada). This linear array transducer has a focal length of 7 mm, lateral resolution of 90 μm, and a axial resolution of 40-μm. Mice were lightly anesthetized with isoflurane during the exams and placed in the supine position on a heated platform with ECG leads and a rectal temperature probe. Longitudinal, transverse, and oblique views of the abdominal cavity were obtained to fully assess for the presence of pathological lesions.

Results (case discussions)

Normal ultrasonographic appearance of the mouse kidney

Ultrasound terminology used to describe images in this report is defined in Table 1. The mouse kidney is unipapillate with a convex outer layer, the cortex, surrounding

Citation: Pathobiology of Aging & Age-related Diseases 2014, **4**: 24932 - http://dx.doi.org/10.3402/pba.v4.24932

an interior layer, the medulla. The inner medulla forms a finger-like renal papilla that projects into and is surrounded by the renal pelvis (12). By ultrasound, the kidney's border is identified by a thin bright echo produced by the renal capsule (Fig. 1a, b). Internally the homogenously gray speckled cortex is hyperechoic (brighter) compared to the neighboring hypoechoic medullary tissue, producing a distinguishable corticomedullary (C:M) border (Fig. 1). Brighter areas may be visible in the center of the medulla, representing peripelvic fat and connective tissues of the renal pelvis and sinus. Most importantly, the area of the renal pelvis is a potential space and should not be expanded with urine and therefore is not visible on ultrasound.

Hydronephrosis and suppurative pyelonephritis

A 2-year-old male B6;129 mouse presented with a draining preputial gland abscess (Fig. 2a). A pre-mortem ultrasound exam detected multiple abnormalities in the kidneys, bladder, and accessory sex glands. A solid 3 mm diameter mass was fixed to the lateral bladder wall and projected into the lumen (Fig. 2b, c). Echogenic debris floated within the lumen and sediment had accumulated on the dependent portion of the bladder wall (Fig. 2b, c). Prominent prostate glands were observed underneath the bladder and a cystic structure filled with anechoic fluid was seen to the right of the lower bladder wall (Fig. 2c). Renal pelvic dilation was apparent as an anechoic space containing echogenic debris in the center of the left kidney (Fig. 2d, e). The kidney showed ultrasonographic features consistent with pyelonephritis including diffuse patchy areas of increased echogenicity within the parenchyma, an indistinct C:M border, and irregular margins (Fig. 2d, e). The preputial gland abscess cultured positive for *Escherichia coli* and *Eneterococcus faecalis*. The urine was positive for leukocytes, protein, and blood but was not submitted for culture. Histological diagnoses included urinary papilloma, cystitis, prostatitis, ureteritis, and severe chronic suppurative pyelonephritis. While prostatitis, cystitis, ureteritis, and bladder masses are all causes of urinary blockage, the renal pelvic dilation observed was likely due to the suppurative pyelonephritis.

The presence of echogenic debris in the dilated pelvis indicates pyonephrosis, an infection within the renal collecting system, which is a complication of pyelonephritis (32). The debris includes inflammatory cells, bacteria, and medullary cells sloughed off of the renal papilla into the pelvic space causing a pelviureteral obstruction (32).

Preputial gland abscesses are common in older mice (15,33). The glands' ducts enter the prepuce, allowing bacterial entry into the urethra, accessory sex glands, bladder, and upper urinary tract. Preputial gland abscesses can thus lead to ascending UTI, secondary infections of accessory glands, and pyelonephritis (16,33). Preputial abscesses are also common causes of inflammatory urethral obstructions that may lead to hydronephrosis (12,16,33). Ascending UTIs are the most common cause of pyelonephritis in small animals, and in man it usually originates from the urethra or the periureteric lymphatics (34,35), with *E. coli* infections associated with the former (36). The ultrasonographic evidence of bladder sediment, the urinalysis results, the presence of a debris filled cystic accessory gland lateral to the bladder, and the histological findings of prostatitis, and ureteritis, suggest this animal had an ascending UTI likely related to the preputial gland abscess. This resulted in ascending pyelonephritis, pyonephrosis, and hydronephrosis.

Cystolithiasis

Ultrasound imaging detected changes consistent with bilateral pyelonephritis, hydronephrosis and cystolithiasis in a 2-year-old male C57BL/6J. Ultrasound images are presented in Fig. 3 and include renal pelvic dilation, medullary atrophy, pyonephrosis, and hyperechoic bladder stones. Findings at necropsy attributed the bilateral ascending pyelonephritis to cystitis. Bladder calculi can be associated with bacterial cystitis in mice (37). Struvite stones resemble white coarse salt grains (37) and may arise secondary to bacterial cystitis when bacteria hydrolyze urea, raising urine pH. Cystolithiasis, pyonephrosis, and proximal ureteral mucosal hyperplasia created favorable conditions for the development of hydronephrosis in this mouse.

Table 1. Common ultrasound terminology

Term	Definition
Echogenicity	Echogenicity refers to a tissue's ability to produce echoes and the resultant characteristic shade of gray it produces on a scale from black to white.
Anechoic	Tissues that are anechoic do not produce echoes and appear black. Fluids, such as urine and blood, are anechoic.
Hyperechoic (echogenic)	Tissues that reflect ultrasound waves strongly are hyperechoic or echogenic, and appear light gray to white.
Hypoechoic	Weaker echo-producing tissues, appearing a darker shade of gray on the grayscale.

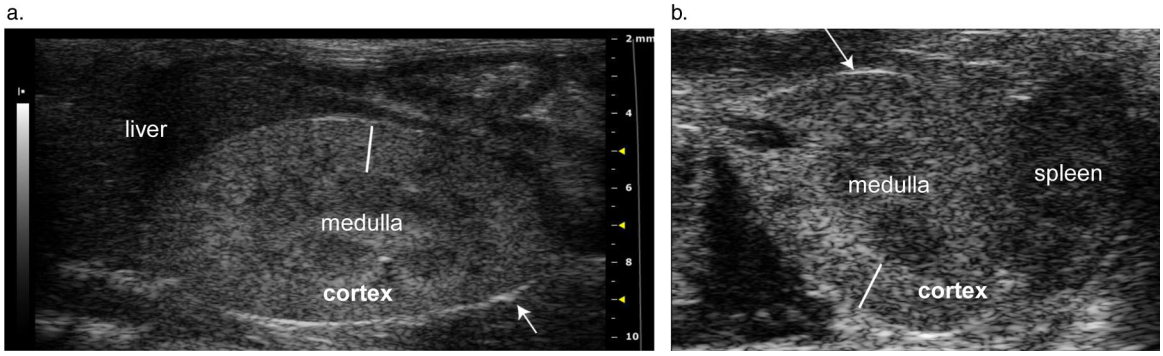

Fig. 1. (a) and (b). Normal longitudinal (a) and transverse (b) 2-D images of the kidney. The longitudinal image is oriented with the animal's head towards the left of the image, while the transverse image shows structures on the left side of the body to the right of the image. Arrows point to a thin bright line representing the echogenic renal capsule. The solid white lines span the renal cortex, which appears hyperechoic to the neighboring medulla.

Hydronephrosis and infiltrative neoplasia

A 2-year-old C3H/HeJ male mouse was diagnosed with bilateral hydronephrosis secondary to infiltrative neoplasia during an abdominal ultrasound exam. The left kidney was enlarged with increased echogenicity and loss of the C:M junction (Fig. 4b–d). The renal pelvis was dilated with anechoic fluid (Fig. 4b–d). The right kidney also showed a loss of internal renal architecture and had a homogenous, hypoechoic echotexture and renal pelvic dilation (Fig. 4e). The cranial border of the right kidney was flattened due to compression from a severely enlarged perirenal lymph node (Fig. 4e). Enlarged, rounded and hypoechoic lymph nodes were seen throughout the abdomen, ranging in size from 9 to 19 mm in length (Fig. 4a–f). The mouse had splenomegaly with multiple hypoechoic nodules (Fig. 4f). Finally, the

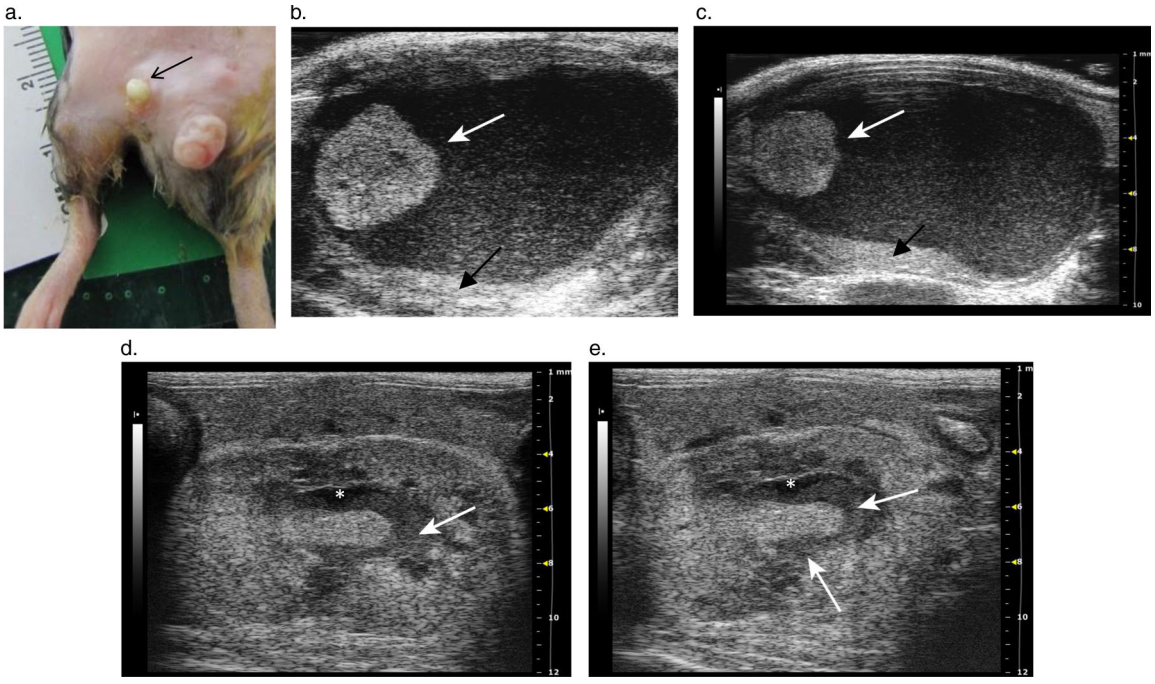

Fig. 2. Hydronephrosis in a mouse with a preputial gland abscess and pyelonephritis. (a) Purulent discharge from a preputial gland abscess (arrow) (b) and (c). 2-D transverse images through the urinary bladder showing a round hyperechoic mass attached to the lateral bladder wall (white arrows). Echogenic debris floats in the bladder lumen and accumulates above the dorsal wall of the bladder (black arrows). The bladder wall is also thickened. In (c), the prostate gland is prominent underneath the bladder and a dilated accessory sex gland is visible dorsolateral to the bladder. (d) and (e). Longitudinal 2-D images of the left kidney with pyelonephritis, pyonephrosis, and hydronephrosis. The urine expanding the renal pelvis appears anechoic on the ultrasound image (asterisk); however, the pelvis also contains echogenic debris (arrows) due to the development of pyonephrosis in the infected kidney. The corticomedullary junction is not visible in the kidney, and there is overall patchy and increased echogenicity within both the cortex and medulla. The renal border adjacent to the dilated pelvis is irregular, due to the erosion of the renal parenchyma.

Citation: Pathobiology of Aging & Age-related Diseases 2014, **4**: 24932 - http://dx.doi.org/10.3402/pba.v4.24932

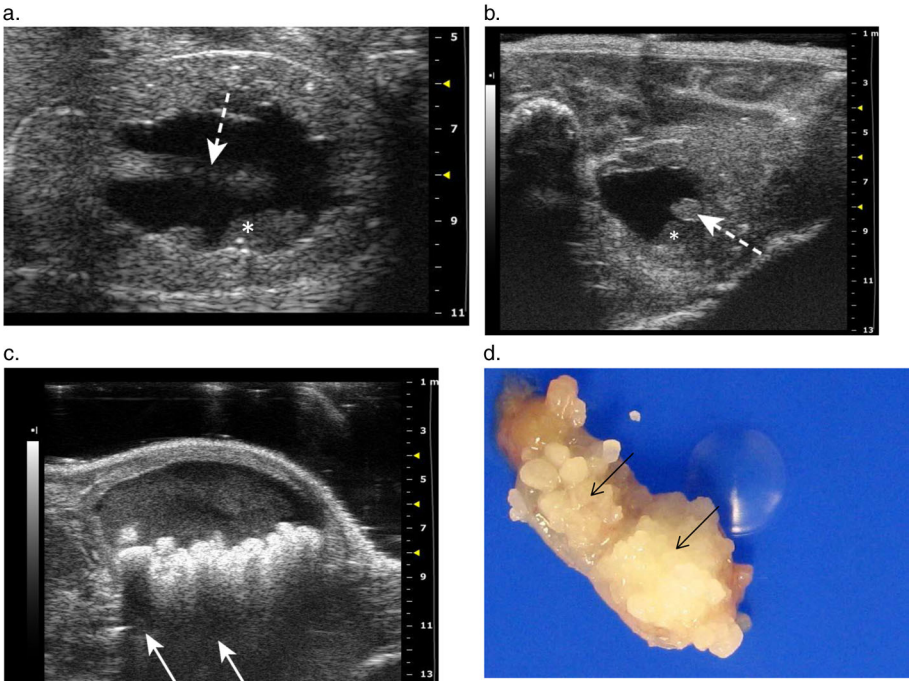

Fig. 3. (a) and (b). Longitudinal (a) and transverse (b) images of the left kidney with hydronephrosis and pyelonephritis. Tissue atrophy is evident producing an irregular and eroded renal parenchymal border along the dilated pelvic space. The renal papilla (dashed arrow) is severely blunted and eroded renal tissue lies in the pelvic space (asterisk). (c) The dependent portion of the bladder lumen is filled with multiple round hyperechoic uroliths. The echogenic stones cause acoustic shadowing (arrow). Hyperechoic debris is visible within the anechoic urine, and the bladder wall is thickened. (d) Image of contents of the bladder, showing numerous white uroliths (arrows).

usually anechoic blood filled lumen of the renal vein was replaced by a uniform, gray, finely speckled echo pattern along its length from the renal hilum to the inferior vena cava (Fig. 4d), consistent with a thrombosis.

Histology of the left kidney revealed infiltration with malignant histiocytes and multinucleated cells and areas of osseous metaplasia. Neoplastic cell invasion of the kidney paralleled the diffuse change in echogenicity and loss of renal architecture on the 2-D ultrasound images. Histology further confirmed that the cause of the abdominal lymphadenopathy and splenic enlargement was due to histiocytic sarcoma (HSC).

HSC is a common neoplasm in aged mice (14) and is a cause of metastatic or hematogenous neoplasia of the mouse kidney (3). This neoplasia is highly malignant, with rapid progression and poor prognosis (14,38). It produces nodular to multifocal infiltrates in affected organs including the liver, spleen, and lymph nodes (14,38). Ultrasonographic appearances of HSC include hypoechoic well circumscribed nodules in the spleen as well as enlarged, rounded and hypoechoic lymph nodes (38,39). The enlarged lymph nodes often displace other structures within the abdomen. In this case, enlarged perirenal lymph nodes distorted the shape of the right kidney (Fig. 4e), and displaced the renal artery and vein cranioventrally as the vessels traveled into the renal hilum (Fig. 4d). Displacement and compression of the ureters from abdominal masses is a cause of hydronephrosis and the widespread malignant lymphadenopathy in this mouse likely contributed to the development of the hydronephrosis. The renal vein thrombosis may be secondary to stasis due to compression from adjacent neoplasia; however, because the vessel lumen is fully expanded along its length and its solid echogenic lumen is continuous with the tumor-infiltrated kidney, it has ultrasonographic features more consistent with a tumor thrombosis. Because the renal vein was not submitted for histological analysis, determination of the type of thrombus was not definitively determined. Suspected tumor invasion of the renal vein and the confirmed widespread tumor infiltration of the kidneys indicate tumor infiltration near the ureteropelvic junction, which likely further contributed to the obstruction to urine flow.

Hydronephrosis and MUS

Ultrasound detected hydronephrosis and lesions consistent with mouse urologic syndrome (MUS) in three male C57BL/6J mice aged 24, 25, and 30 months. In addition to renal enlargement and renal pelvic dilation (Fig. 5d, 6c), all mice had engorged seminal vesicles identified as large, sacculated tubular structures distended with anechoic fluid and a thick hyperechoic material (Fig. 5d, 6a–c). The enlarged seminal vesicles originated near the bladder and occupied 2/3 of the abdominal cavity; extending over the cranial poles of the kidneys to the caudal borders of the liver. At necropsy, the seminal vesicles contained white, gray, or brown (Fig. 5c); and watery, hemorrhagic,

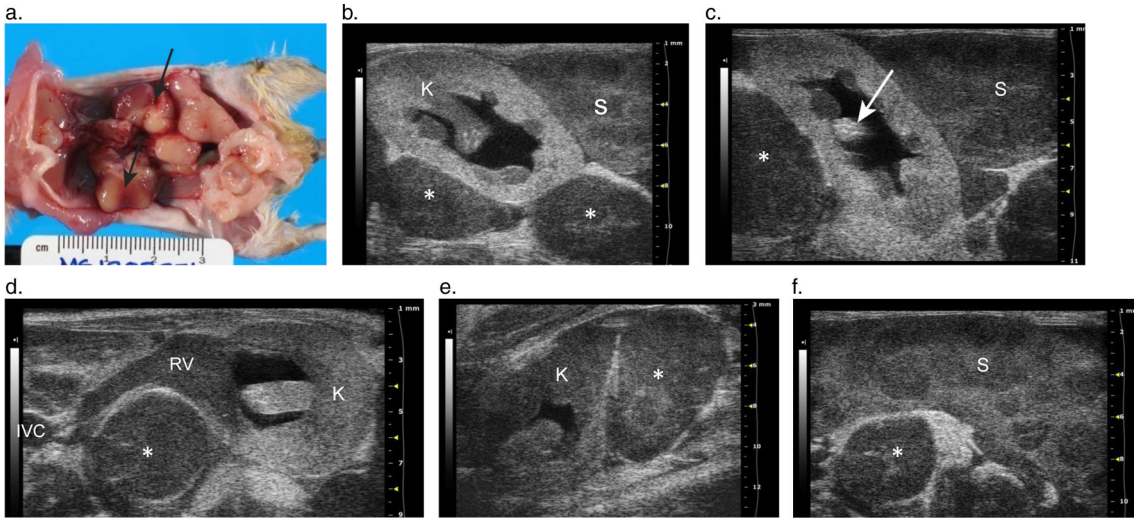

Fig. 4. Images from a C3H/HeJ mouse with histiocytic sarcoma. (a) Gross pathologic lesions in the C3H/HeJ mouse with histiocytic sarcoma showing widespread lymphadenopathy. Tan nodules (lymph nodes) are seen effacing the kidneys (arrows) and the multiple enlarged tan lymph nodes are prominent throughout the caudal abdomen. (b) 2-D ultrasound image through the left kidney and spleen showing neoplastic infiltration of the spleen (S), kidney (K) and lymph nodes (asterisk) by histiocytic sarcoma. The renal pelvis is dilated, and the renal parenchyma has homogenous and diffusely increased echogenicity. The lymph nodes (asterisk) and spleen (S) are enlarged with prominent multifocal dark nodules scattered throughout the interior of the spleen. (c) Another view of the left kidney flanked between the spleen (S) and a large lymph node (asterisk). A section of papilla is visible showing intensely hyperechoic foci consistent with the histological finding of osseous metaplasia (arrow). (d) 2-D transverse image of the left kidney shows renal pelvic dilation and tumor thrombosis of the renal vein. The lumen of the renal vein (RV) is solid, producing gray echoes of similar echogenicity to the enlarged lymph node (asterisk) due to suspected infiltration of the vessel with neoplastic cells. The infiltrated renal vein is traceable along its length from the hilum to the inferior vena cava (IVC) and is displaced ventrally by the enlarged lymph node (asterisk). (e) The right kidney (K), and a severely enlarged perirenal lymph node (asterisk) that is distorting the cranial pole of the kidney. The right kidney also exhibits mild renal pelvic dilation. (f) Splenomegaly, with multifocal hypoechoic nodules.

or thick inspissated material. Bladder distension was also evident on ultrasound, with dense hyperechoic material observed on the dependent portion of the bladder wall in two cases (Fig. 5b). This soft tan/brown bladder coagulum (Fig. 5a) was composed of erythrocytes and a proteinaceous material, consistent with an origination from the seminal vesicles.

Histological findings included renal tubular dilatation, renal papillary necrosis and hemorrhage, and seminal vesicle inflammation. Two mice had intraluminal hemorrhagic bladder coagula that caused acute obstruction of the urinary bladder with bladder distension, bilateral hydronephrosis, renal ductal ectasia and papillary necrosis. The third mouse had severe bilateral seminal vesicle dilation with right-sided *Enterobacter cloacae* culture positive vesiculitis, right-sided unilateral hydroureter (Fig. 6a–c), and hydronephrosis with renal tubular dilatation and non-suppurative interstitial nephritis without evidence of ureteritis or a bladder coagulum.

Despite minor differences, the above cases share features of MUS. MUS is caused by an obstruction to urine flow from the bladder by proteinaceous material derived from the accessory male sex glands (14,37). Findings associated with this condition in mice include bladder dilation, hydronephrosis, hemorrhages and inflammation in genitourinary tissues, and abnormal secretions from the accessory sex glands (37). Two of the cases developed bilateral hydronephrosis from an obstructive uropathy caused by a coagulum of seminal vesicle origin in the bladder neck. This condition is common in C57BL mice (14,37) and the male STR/N strain which also develops hydronephrosis, occlusion of the urethral sinus and suppurative vesico-urethritis (12,40). The third case with the infected seminal vesicle had unilateral hydroureter and hydronephrosis without a visible obstruction. As enlargement of the seminal vesicles is common in aged C57BL/6 mice, often confused with abdominal tumors at physical exam (15), the seminal vesicle may act as a space occupying mass kinking the ureter. Urine retention can also occur with accessory gland inflammation, as reported in an aged mouse with unilateral hydronephrosis and seminal vesicle infection (15).

Spontaneous hydronephrosis

Marked left-sided hydronephrosis was detected in a 24-month-old female KO mouse on a C57BL6 background during abdominal ultrasound. The cranial kidney appeared as a large anechoic fluid filled sac with little remaining parenchymal tissue (Fig. 7b, c). The longitudinal view of the kidney showed extreme pelvic dilation with distant enhancement, parenchymal loss, and alteration of renal tissue architecture (Fig. 7c). Postmortem exam

Citation: Pathobiology of Aging & Age-related Diseases 2014, **4**: 24932 - http://dx.doi.org/10.3402/pba.v4.24932

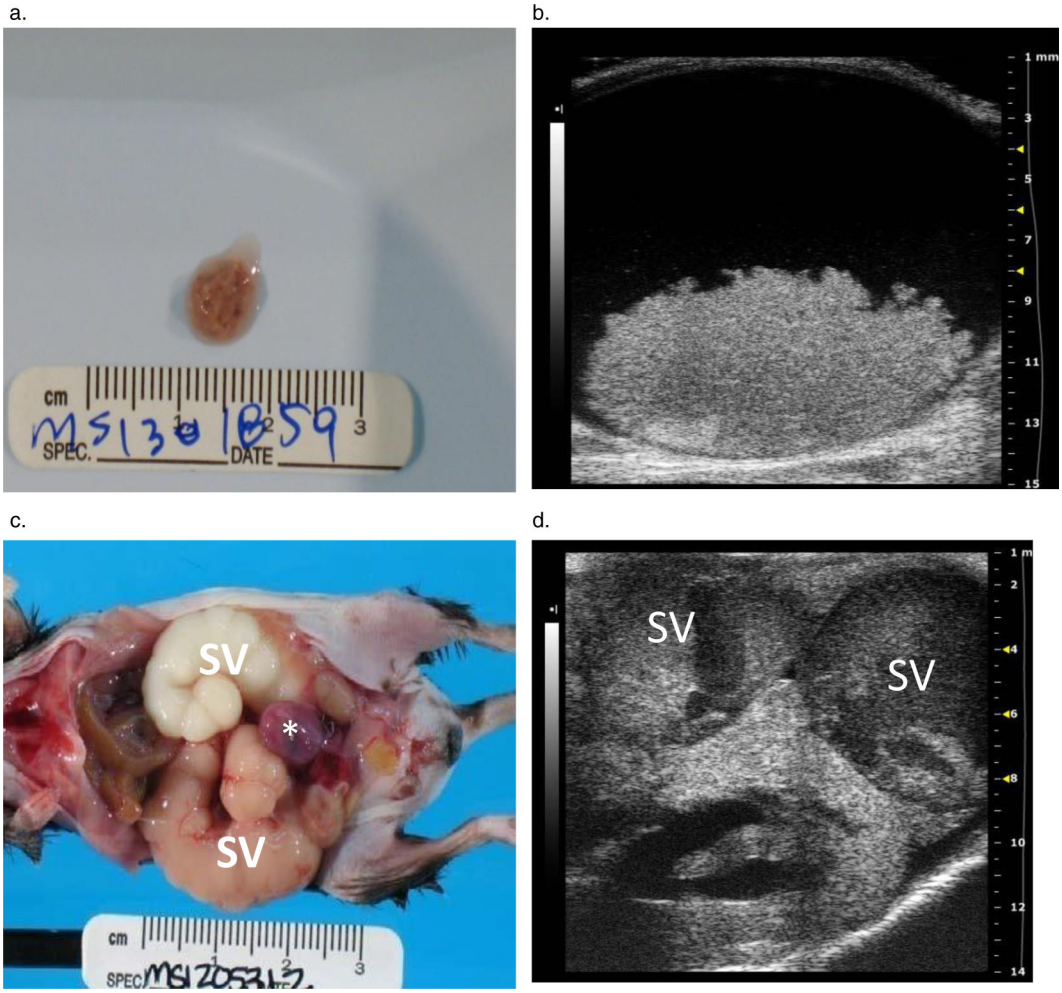

Fig. 5. Images from male C57BL/6J mice with mouse urologic syndrome. (a) A coagulum of blood and proteinaceous material in the bladder of a mouse with bilaterally enlarged hemorrhagic seminal vesicles. The material originated from the seminal vesicles and caused an acute, severe bladder outlet obstruction. (b) The transverse 2-D image of the bladder shown in (a) shows the obstructive seminal vesicle coagulum in the bladder lumen. The large (6 mm × 12 mm) hyperechoic mass is clearly visible on the floor of the bladder. (c) Urinary tract and reproductive gland lesions in a second male mouse, including enlarged tan and white seminal vesicles (SV) filled with seminal gland secretions and a hemorrhagic urinary bladder (asterisk). (d) A corresponding transverse 2-D ultrasound image for (c) shows the severely distended, sacculated seminal vesicle (SV) containing echogenic material overlying the left hydronephrotic kidney.

confirmed left-sided hydronephrosis (Fig. 7a), hydroureter, lymphocytic inflammatory infiltration of the hydronephrotic kidney and lymphocytic aggregates in the left ureter and cranial pole of the bladder. A urinary tract obstruction was not identified, despite the presence of lymphocytic inflammation around the left dilated ureter. Furthermore, histology revealed multiple small residual glomeruli, spaced closely together along the periphery of the cortex in the hydronephrotic kidney, (Fig. 7f) with tubular hypoplasia, and moderate lymphocytic interstitial infiltrate (Fig. 7e, f).

This mouse had ureteritis with ureteral dilation on the side of the affected kidney. Ureteral inflammation and fibrosis can lead to acquired hydronephrosis, however, the lumen remained patent along the length of the ureter and no inflammatory obstructions were identified. The histological identification of small glomeruli lacking associated tubular elements, however, suggests a primary congenital spontaneous hydronephrosis. The lack of association between glomeruli and tubular elements, and tubular hypoplasia indicate a developmental abnormality occurring during mesenchymal differentiation and nephrogenesis of the metanephric kidney (41). It is noteworthy that in addition to detecting the dilated ureter in this case of hydronephrosis, a round dilatation with a thin echogenic wall was observed protruding into the bladder lumen near the neck of the bladder, consistent with an ureterocele (Fig. 7d). Ureteroceles are a congenital lesion of the urinary tract and a cause of hydroureter and hydronephrosis in man (42). They are thin walled

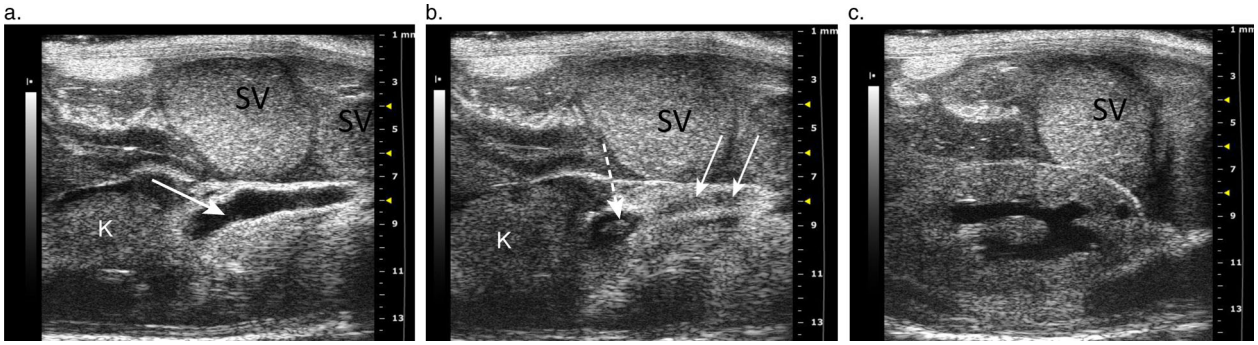

Fig. 6. Serial longitudinal images, medial to lateral, trace a dilated ureter (arrow) into the renal hilum of a mouse with renal pelvic dilation, seminal vesicle gland infection, and mouse urologic syndrome. (a) Arrow points to the lumen of a dilated tubular structure, the right ureter, located distomedially to the right kidney. (b) The ureter (solid arrow) is followed laterally, as it enters the anechoic space of the renal pelvis. A small portion of the renal papilla is visible within the pelvis (dashed arrow). (c) Longitudinal 2-D image of the right kidney with renal pelvic dilation and a small well demarcated cortical cyst. Note: the thick echogenic material in the dilated seminal vesicles (SV) above the kidney and ureter, which contained inspissated seminal gland fluid that cultured positive for *Enterobacter cloacae*.

cystic protrusions of the distal ureter into the lumen of the bladder through the ureteral orifice, producing an obstruction in the affected ureter (43). Ureteroceles have not been previously reported in mice and the suspected ureterocele was not confirmed at necropsy; however, we have subsequently confirmed a ureterocele with a similar ultrasonographic appearance in a young mouse with congenital hydronephrosis.

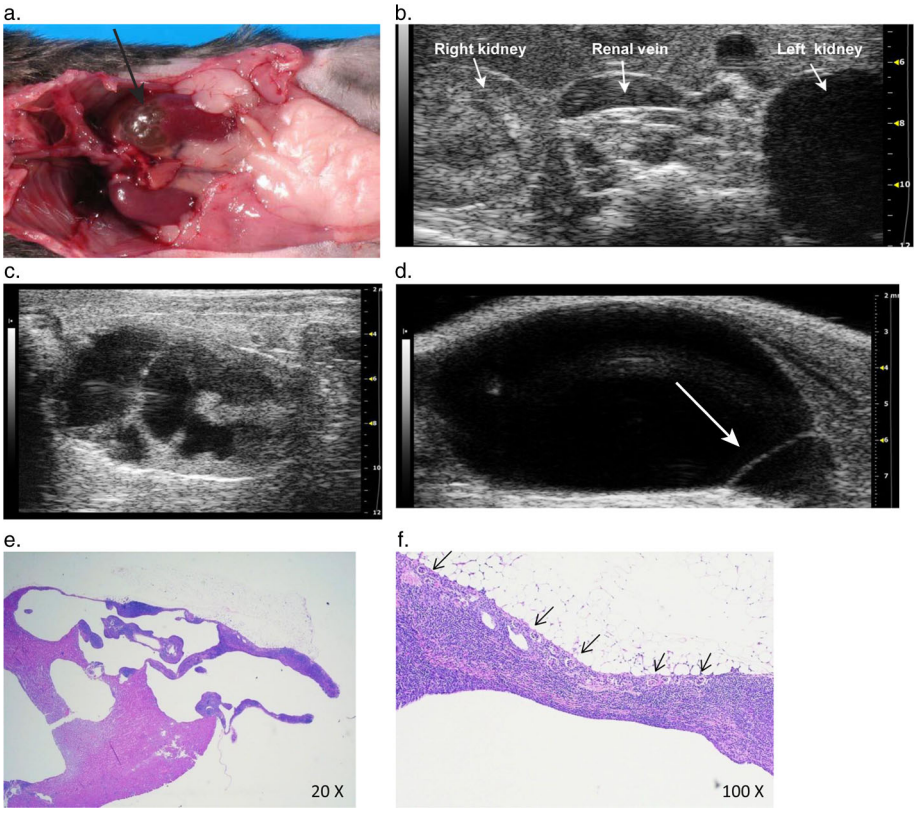

Fig. 7. Severe unilateral hydronephrosis in the left kidney. (a) The cranial pole of the left kidney (arrow) is thin walled and appears translucent due to severe urine distension and attenuation of renal parenchyma from hydronephrosis. (b) Transverse 2-D ultrasound image showing the unaffected right kidney compared to the thin-shelled fluid filled cranial pole of the left kidney that is completely void of detectable cortical tissue. (c) 2-D longitudinal image of the left kidney with severe renal pelvic dilation, and renal parenchymal atrophy with distortion and loss of the normal renal architecture. (d) Longitudinal image of the urinary bladder showing a thin walled cystic structure (arrow) protruding into the base of the bladder, consistent with an ureterocele. (e) Histological image showing the hydronephrotic portion of the cranial pole of the kidney. (f) Histological image showing multiple small glomeruli (arrows) along the periphery of the affected cortex with an associated moderate lymphocytic interstitial infiltrate.

Citation: Pathobiology of Aging & Age-related Diseases 2014, **4**: 24932 - http://dx.doi.org/10.3402/pba.v4.24932

Table 2. Summary of the cases of acquired hydronephrosis described in manuscript

Signalment	Primary underlying etiology		Ultrasonographic and pathological findings
Case 1 24 mo. male B6;129	Pyelonephritis	Kidney	Pyelonephritis, pyonephrosis, hydronephrosis (bilateral)
		Bladder	Bacterial cystitis, luminal sediment, urinary papilloma
		Other	Preputial gland abscess, prostatitis, ureteritis, ascending UTI
Case 2 24 mo. male C57BL/6J	Cystolithiasis	Kidneys	Bilateral pyelonephritis, hydronephrosis
	Pyelonephritis	Renal pelvis	Luminal and mucosal neutrophilc infiltrate
		Ureters	Villous mucosal hyperplasia of proximal left ureter
		Bladder	Calculi (struvite stones suspected but not sent for analysis), bacterial cystitis
		Other	Ascending urinary tract infection
Case 3 24 mo. male C3H/HeJ	Infiltrative multi-organ abdominal neoplasia (histiocytic sarcoma)	Kidneys	Effacement by enlarged perirenal lymph nodes, infiltration of parenchyma by neoplastic cells, osseous metaplasia, chronic nephropathy, mild bilateral hydronephrosis
		Renal vein	Tumor thrombus and displacement by adjacent enlarged lymph nodes
		Lymph nodes	Enlargement and neoplastic cell infiltration of mediastinal, perirenal, gastric, and pancreaticoduodenal lymph nodes
		Spleen	Enlargement with multifocal to coalescing nodules
Case 4 24 mo. male C57BL/6J	Mouse urologic syndrome	Kidneys	Bilateral mild hydronephrosis with renal pelvic necrosis and tubular distension
		Bladder	Obstruction with hemorrhagic coagulum and severe distension.
		Seminal Ves	Severe bilateral distension and hemorrhage.
		Preputial glands	Suppurative adenitis
Case 5 25 mo. male C57BL/6J	Mouse urologic syndrome	Kidneys	Bilateral mild hydronephrosis with tubular dilatation, and renomegaly
		Bladder	Luminal hemorrhagic coagulum
		Seminal Ves	Bilateral enlargement with the right side showing brown discoloration of contents. Bilateral adenitis
Case 6 30 mo. male C57BL/6J	Mouse urologic syndrome	Kidneys	Unilateral right-sided mild hydronephrosis, bilateral tubular dilatation, and mild renal enlargement
		Ureters	Mild right-sided hydroureter
		Seminal Ves	Bilateral enlargement with brown inspissated material (left) and *Enterobacter cloacae* + brown watery material (right). Bilateral adenitis
		Bladder	Echogenic material in lumen
Case 7 24 mo. female C57BL/6J background	Spontaneous hydronephrosis and ureteritis	Kidneys:	Unilateral severe left-sided hydronephrosis. Severe cranial parenchymal attenuation and moderate caudal parenchymal attenuation. Tubular hypoplasia
		Ureters:	Left ureteral dilation with adventitial lymphocytic aggregates
		Bladder:	Adventitial lymphocytic aggregates at cranial pole and hemosiderin-laden macrophages

Note: mo = month, seminal ves = seminal vesicles.

Spontaneous hydronephrosis represents the development of hydronephrosis with no apparent cause, and may be congenital. In fact, spontaneous hydronephrosis is one of the most frequently reported congenital lesions of the mouse kidney (3). It is unlikely that the condition was related to the deleted gene in this female KO mouse, as none of the other KO mice in the study ($n = 30$) developed hydronephrosis.

An autosomal recessive spontaneous hydronephrosis has been reported in adult C57BL/6 and C57L mice (3,8) with no apparent cause (12), although none of the littermates and non-littermate siblings of this case developed the condition. Other causes for spontaneous hydronephrosis in mice include: obstructions occurring secondary to partial constriction of the ureter by the spermatic artery (2), abnormal ureteral venation causing

pressure on the ureter (21), or inhibition of ureteric muscular contractions secondary to genital artery position (5). Functional impairments to urine transport due to a neuronal or muscular pathology impairing pyeloureteral peristalsis (13) is another possibility.

The severe hydronephrosis in this aged mouse was likely attributable to a congenital etiology rather than acquired from ureteral inflammation. Although many congenital anomalies in mice are lethal, lesions may be detected in aged animals with milder expression of a genetic trait (12). Furthermore, adult mice with unilateral spontaneous hydronephrosis can remain asymptomatic as the unaffected kidney is able to compensate. This case highlights the importance of considering congenital causes for lesions occurring in aged animals.

Discussion

This paper presents the most current and comprehensive report of acquired hydronephrosis in naturally aging mice. High-resolution ultrasound imaging enabled the pre-mortem detection of hydronephrosis as well as the identification of concurrent abdominal lesions involved in the underlying etiologies associated with this condition in mice. We have reported seven cases of hydronephrosis in aged laboratory mice detected by ultrasound imaging. The underlying etiologies included: pyelonephritis secondary to a preputial gland abscess and ascending UTI; cystolithiasis, infiltrative abdominal neoplasia with invasion of the renal pelvis, hilum, and parenchyma and surrounding lymph nodes; MUS, and a case of spontaneous hydronephrosis with ureteritis. The ultrasonographic and pathologic findings from the seven case reports are summarized in Table 2.

We retrospectively reviewed 149 additional abdominal ultrasound exams conducted in our facility from 2011 to 2013 (Tables 3–5) to determine the incidence of the underlying etiologies associated with urinary tract obstructions in aging mice (Fig. 8) and the frequency of concurrent renal pelvic dilation (Fig. 9). These mice were being housed to age naturally by the NHLBI Murine Phenotyping Core, and were imaged at the onset of signs of morbidity for pre-mortem detection of pathological lesions. Fig. 9a includes data from mice with renal pelvic dilation detectable on ultrasound and not easily viewed by gross examination, but significant enough to be considered mildly hydronephrotic (expanded renal pelvis measured $>14\%$ but $<30\%$ total renal diameter with renal pelvic dilation alone or with mild narrowing of the renal papilla). These mildly hydronephrotic cases may represent early, acute, or incomplete urinary blockages. Fig. 9b includes data from mice with dilation corresponding to an expanded renal pelvic diameter measuring $>30\%$ the total kidney diameter on ultrasound and qualifying for a grade of moderate (pelvic dilation with significant loss of renal medulla), and severe hydronephrosis (pelvic dilation and significant loss of medullary and cortical parenchyma).

Table 3. Mouse strains included in the retrospective review of abdominal ultrasound scans conducted from fall 2011 to fall 2013

Strain	Females	Males
C67BL/6J	3	35
CAST/EiJ	5	0
Swiss Webster	5	5
B6;129	3	17
Myoglobin$^{+/+}$	5	8
Slc26a6$^{-/-}$	1	5
BALB/cJ	32	0
AKR/J	1	2
FVB/N	2	6
SJL/J	1	3
C3H/HeJ	0	5
CD-1	0	2
AKR/J	0	3

Results from the retrospective review (Tables 4 and 5) combined with the seven presented case reports reveal that MUS (10.3% of males) and widespread abdominal neoplasia (20.5% of both males and females) were the two most common conditions with 70% of the cases of MUS occurring with concurrent renal pelvic dilation versus 44% of the abdominal neoplasia cases. Six out of seven mice with both MUS and renal pelvic dilation had enlargement of the seminal vesicles and ultrasonographic evidence of a coagulum within the bladder lumen, while one mouse had enlarged seminal vesicles and a urethral coagulum with urethral dilation. As the bladder or urethral coagula, and the renal pelvic and urethral dilation were detected during the imaging of live mice, this condition cannot be considered an agonal event. It is noteworthy to mention that seminal vesicle adenitis and enlargement was very frequent in aged males (19–31 months of age), affecting 57% of C57BL/6Js and 50% of FVB/N males and this condition may be related to the development of MUS, which was also more frequent in C57BL/6J and FVB/N males.

HSC (45%) and lymphoma (33%) were the most frequently reported type of all cases of widespread abdominal neoplasia with 47 and 36%, respectively, of mice with HSC and lymphoma presenting with renal pelvic dilation. Of the mice with HSC, lymphoma and renal pelvic dilation, 92% also had widespread abdominal lymphadenopathy; suggesting that enlarged lymph nodes around the kidney or ureters may obstruct urine flow. In addition, 69% of the cases with HSC, lymphoma and renal pelvic dilation had neoplastic cell infiltration in the kidney.

Citation: Pathobiology of Aging & Age-related Diseases 2014, **4**: 24932 - http://dx.doi.org/10.3402/pba.v4.24932

Table 4. Summary of a retrospective review of ultrasound exams in 149 mice and the occurrence of abdominal neoplasia and the presence of renal pelvic dilation

Multi-organ abdominal neoplasia			
Tumor type	Signalment	Organs affected in abdomen	Renal pelvic dilation
Histiocytic sarcoma (HSC)	Myoglobin$^{+/+}$ F, 30 mo.	Liver, spleen, lymph nodes	No
	C57BL6 F, 31 mo.	Liver, spleen, kidney, reproductive tract, lymph nodes	No
	C57BL6 F, 18 mo.	Liver, spleen, pancreas, lymph nodes	No
	SJL/J F, 11 mo.	Liver, lymph nodes	Yes, bilateral
	C57BL/6J M, 14 mo.	Liver, spleen	No
	C3H/HeJ M, 28 mo.	Liver, abdominal lymph nodes	No
	C57BL/6J M, 23 mo.	Liver, spleen with bilateral glomerulopathy	Yes, right side
	C3H/HeJ M, 24 mo.	Liver, spleen, kidneys, ureters, lymph nodes	Yes, bilateral
	C57BL/6J M 27 mo.	Liver, spleen, lymph nodes	No
	C57BL/6J M, 27 mo.	Liver, spleen, pancreas, mesentery, lymph nodes	No
	Swiss Webster M, 19 mo.	Liver, spleen, kidneys, lymph nodes	Yes, bilateral
	B6;129 M, 24 mo.	Liver, pancreas, stomach, bladder, lymph nodes	No
	SJL/J M, 11 mo.	Liver, spleen, pancreas, lymph nodes	Yes, left side
	SJL/J M, 11 mo.	Spleen, liver, pancreas, lymph nodes with neoplastic cell infiltrates in renal tubules	Yes, unilateral side not documented
Lymphoma	Swiss Webster F, 21 mo.	Liver, spleen, kidneys, lymph nodes	Yes, left side
	Myoglobin$^{+/+}$ F, 30 mo.	Spleen, kidneys, lymph nodes	Yes, right side
	B6;129 F, 27 mo.	Liver, spleen, lymph nodes	No
	AKR/J F, 11 mo.	Spleen, kidneys, reproductive tract, lymph nodes	No
	Swiss Webster M, 10 mo.	Spleen, liver, kidney, pancreas, lymph nodes	Yes, left side
	Swiss Webster M, 14 mo.	Abdominal lymph nodes	No
	Swiss Webster M, 16 mo.	Spleen, liver, abdominal lymph nodes	No
	Slc26a6$^{-/-}$ M, 24 mo.	Spleen, liver, lymph nodes	No
	FVB/N M, 20 mo.	Spleen, liver, kidneys, stomach, pancreas, mesentery, gall bladder, testes, epididymis, SVs, preputial glands	No
	Myoglobin$^{+/+}$ M, 27 mo.	Spleen, liver, kidneys, pancreas, lymph nodes	Yes, bilateral
	AKR/J M, 11 mo.	Spleen, liver, pancreas, kidneys, lymph nodes	No
HSC and Lymphoma	B6;129 F, 31 mo.	Liver, spleen, pancreas, lymph nodes	Yes, left side
	BALB/cJ F, 24 mo.	Spleen, lymph nodes, perirenal mass	Yes, bilateral
	Myoglobin$^{+/+}$ M, 26 mo.	Spleen, liver, mesentery, perirenal masses, and Abdominal lymph nodes (pleomorphic lymphoma with histiocytic infiltrates, or mixed tumor)	No
Hemangiosarcoma	CAST/EiJ F, 27 mo.	Liver, spleen	No
Other neoplasia	Swiss Webster F, 20 mo.	Ovarian granulosa cell tumor, mammary adenosarcoma, with severe bilateral nephropathy	Yes, left side
	Swiss Webster M, 14 mo.	Myelogenous leukemia in spleen, liver, blood vessels.	No
	Myoglobin$^{+/+}$ M, 22 mo.	Bladder carcinoma, liver adenoma and carcinoma	No

mo = month, HSC = histiocytic sarcoma.

All mice with pyelonephritis developed pyonephrosis with hydronephrosis, but the condition was infrequent, only affecting two animals. Cystolithiasis was common in Slc26a6$^{-/-}$ mice as these mice have a phenotype of increased urine oxalate excretion (44). Finally, 22.2% of all mice with uroliths presented with a hydronephrotic kidney. Therefore, based on the seven cases presented in this report, and the subsequent retrospective survey of 149 other abdominal imaging exams and pathology reports, abdominal neoplasia and MUS were the most common underlying etiologies leading to the development of acquired hydronephrosis in aging laboratory mice.

As laboratory mice are important research models for the study of renal physiology and disease processes, it is important to recognize and understand naturally occurring disease processes that impact them throughout

Table 5. Summary of a retrospective review of ultrasound exams in 149 mice showing the occurrence of common underlying etiologies involved in urinary tract obstructions in mice and the presence of renal pelvic dilation

	Signalment	Necropsy and ultrasound findings	Renal pelvic dilation
Mouse urologic syndrome	C57BL/6J M, 24 mo.	Enlarged SVs (bilateral), echogenic bladder coagulum.	Yes
	C57BL/6J M, 24 mo.	Enlarged SVs (bilateral) with adenitis and culture + for *E. cloacae and Pseudomonas aeruginosa* echogenic coagulum in bladder	No
	C56BL/6J M, 25 mo.	Enlarged SVs (bilateral), bladder distension with luminal echogenic material, urethral dilation	Yes, bilateral
	FVB/N M, 22 mo.	Enlarged SVs (bilateral), bladder distension with thick echogenic material in lumen	No
	FVB/N M, 24 mo.	Enlarged SVs (bilateral), luminal hemorrhage bladder, cystic preputial and bulbourethral glands, and paraphymosis	No
	C57BL/6J M, 29 mo.	Enlarged SVs, bladder distension with echogenic debris, urethral dilation with echogenic debris (in addition had histiocytic sarcoma of the spleen)	Yes, bilateral
	B6;129 M, 29 mo.	Enlarged SVs, bladder distension with echogenic coagulum.	Yes, right side
Cystolithiasis	Signalment	Necropsy and ultrasound findings	Renal pelvic dilation
	BALB/cJ F, 21 mo.	Bladder calculi	No
	Slc26a6$^{-/-}$ KO M, 20 mo.	Calcium oxalate calculi in bladder and renal cortical mineralization	No
	Slc26a6$^{-/-}$ M, 24 mo.	Calcium oxalate calculi in bladder	No
	Slc26a6$^{-/-}$ M, 26 mo.	Calcium oxalate calculi in bladder	No
	Myoglobin$^{+/+}$ M, 24 mo.	Bladder calculi with *Proteus mirabilis* in lumen	No
	Slc26a6$^{-/-}$ KO 3	Bladder calculi (calcium oxalate)	No
	Myoglobin$^{+/+}$ M, 24 mo.	Bladder calculi, urine culture + for *Proteus mirabilis*	Yes
	Slc26a6$^{-/-}$ M, 35 mo.	Bladder calculi, calcium oxalate	No
Spontaneous hydronephrosis	Signalment	Concurrent pathological findings	Renal pelvic dilation
	CAST/EiJ F, 26 mo.	Splenic follicular hyperplasia	Yes, right side
Other	Signalment	Related pathological conditions	Renal pelvic dilation
	C57BL6/J M, 12 mo.	Inguinal testicular herniation, preputial keratin plug	Yes, bilateral

mo. = month, SVs = seminal vesicle.

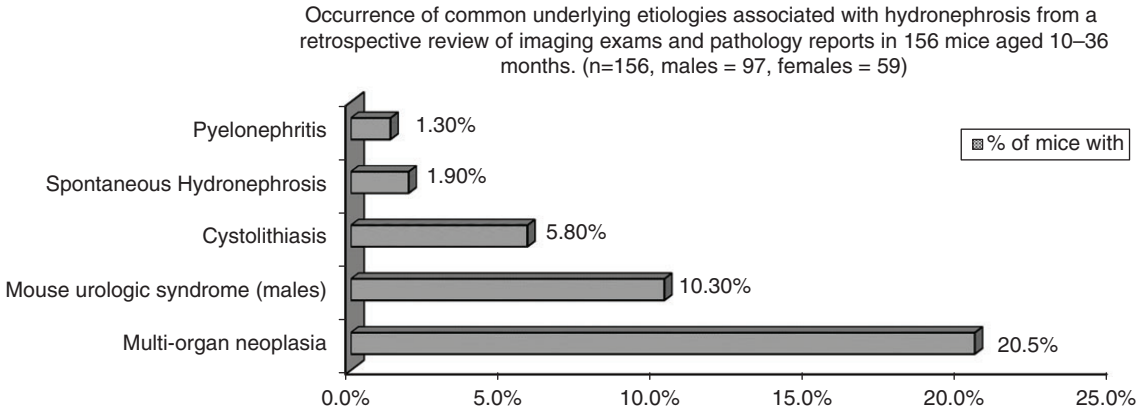

Fig. 8. Results from the retrospective review of imaging exams and pathology reports from 156 mice aged 10–36 months. Graph reports the percentages of all mice that were diagnosed with one of five common underlying conditions associated with acquired hydronephrosis in mice and include both mice with and without renal pelvic dilation.

Citation: Pathobiology of Aging & Age-related Diseases 2014, **4**: 24932 - http://dx.doi.org/10.3402/pba.v4.24932

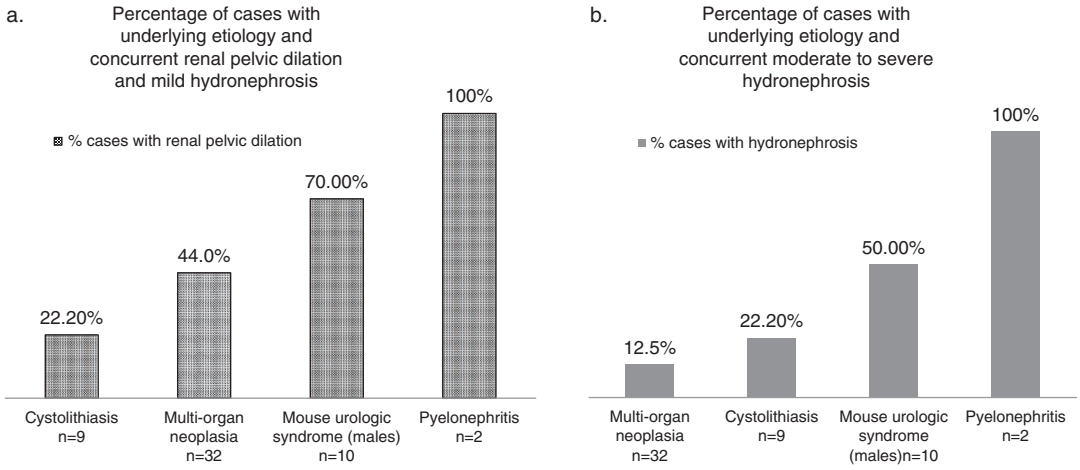

Fig. 9. Results from the retrospective review of imaging exams and pathology reports from 156 mice aged 10–36 months. (a) Percentages of cases for designated etiologies with concurrent renal pelvic dilation and mild hydronephrosis observed on ultrasound (expanded renal pelvic space measured > 14% of total diameter of kidney from transverse image near renal hilum). (b) Percentages of cases for designated etiologies with concurrent unilateral or bilateral moderate to severe hydronephrosis diagnosed at imaging (renal pelvis space expanded > 30% of total width of kidney in transverse image and with significant renal parenchymal loss).

life. We have used abdominal ultrasound imaging to document diverse pathologies that arise during aging and can result in the development of acquired hydronephrosis in aged laboratory mice. The use of high-frequency ultrasound provides high-resolution images, yields valuable pre-mortem clinical information, is minimally invasive and efficient, and is a valuable tool for documenting experimental and natural disease processes occurring in research animals. Furthermore, serial examinations can be performed at multiple time points in the same animal, enabling the study of disease progression and the ability to follow responses to treatments and interventions over time. Ultrasound imaging can also obtain functional measurements and calculations providing researchers with in vivo physiological data, such as cardiac ejection fraction, or renal artery pulsatility and resistivitiy indices. Thus ultrasound imaging is a valuable supplement to postmortem necropsies and histopathological examinations, and increases the information acquired from a single animal. High-frequency ultrasound imaging is an ideal tool for in vivo documentation and study of aging associated pathological processes in laboratory mice.

Acknowledgements

We thank Rachel Fleischman, Kristen Kuzma, and Jorge Chavez for providing gross pathology images; Annie Merriweather and Chris King for histologic preparations; the NIH Division of Veterinary Resources building 14F animal facility staff for animal care; Drs. Mark Knepper and Joe Chou for review of manuscript, and Dr. James Hawkins, Animal Program Director of NHLBI, NIH for animal program support.

Conflict of interest and funding

The NIH Intramural Research Program supported this work. The authors declare no conflicts of interest.

References

1. Mannen H, Tsuji S, Goto N. Influence of chronic oestrogen treatment on severity of hydronephrosis in inbred DDD mice. Lab Anim. 1993; 27: 124–30.
2. Nakajima Y, Imamura K, Onodera T, Motoi Y, Goto N. Hydronephrosis in the inbred mouse strain DDD. Lab Anim. 1983; 17: 143–7.
3. Seely JC. Kidney. In: Maronpot RR, Boorman GA, Gaul BW, editor. Pathology of the mouse. Vienna, IL: Cache River Press; 1999, p. 207–234.
4. Takahashi N, Chernavvsky DR, Gomez RA, Igarashi P, Gitelman HJ, Smithies O. Uncompensated polyuria in a mouse model of Bartter's syndrome. Proc Natl Acad Sci U S A. 2000; 97: 5434–9.
5. Taylor DM, Fraser H. Hydronephrosis in inbred strains of mice with particular reference to the BRVR strain. Lab Anim. 1973; 7: 229–36.
6. Warner NL. Spontaneous hydronephrosis in the inbred mouse strain NZC. Aust J Exp Biol Med Sci. 1971; 49: 477–86.
7. Couture-Haws L, Harris MW, McDonald MM, Lockhart AC, Birnbaum LS. Hydronephrosis in mice exposed to TCDD-contaminated breast milk: identification of the peak period of sensitivity and assessment of potential recovery. Toxicol Appl Pharmacol. 1991; 107: 413–28.
8. Horton CE, Jr., Muriel TD, Jacobs JB, Bernstein GT, Retik AB, Mandell J. Congenital progressive hydronephrosis in mice: a new recessive mutation. J Urol. 1988; 140: 1310–15.
9. Ninomiya H, Inoma T, Ogihara K. Obstructive uropathy and hydronephrosis in male KK-Ay mice: a report of cases. J Vet Med Sci. 1999; 6(1): 53–7.
10. Silverstein E, Sokoloff L, Mickelsen O, Jay GE, Jr. Primary polydipsia and hydronephrosis in an inbred strain of mice. Am J Pathol. 1961; 38(2): 143–59.
11. Wright JR, Lacy PE. Spontaneous hydronephrosis in C57BL/KsJ mice. Comp Pathol. 1988; 99: 449–54.
12. Dunn TB. Renal disease of the mouse. In: Cotchin E, Roe FJC, editor. Pathology of laboratory rats and mice. Oxford: Blackwell Scientific; 1967, p. 149–179.
13. McDill BW, Li S-Z, Kovach PA, Ding L, Chen F. Congenital progressive hydronephrosis (cph) is caused by an S256L mutation in aquaporin-2 that affects its phosphorylation and

apical membrane accumulation. Proc Natl Acad Sci. 2006; 103: 6952–7.
14. Percy DH, Barthold SW. Pathology of laboratory rodents and rabbits. 2nd ed. Oxford: Blackwell; 2007.
15. Pettan-Brewer C, Treuting PM. Practical pathology of aging mice. Pathobiol Aging Age Relat Dis. 2011;1.
16. Tucker MJ, Baker DEC. Diseases of specific pathogen-free mice. In: Cotchin E, Roe JCF, editor. Pathology of laboratory rats and mice. Oxford: Blackwell Scientific; 1967, p. 787–823.
17. Zurcher C, van Zwieten MJ, Solleveld HA, Hollander CF. Aging research. In: Foster JL, Small JD, Fox JG, editor. The mouse in biomedical research: volume IV. New York: Academic Press; 1982, p. 11–35.
18. Carter TC. The genetics of luxate mice. III. Horseshoe kidney, hydronephrosis and lumbar reduction. J Genet. 1953; 51(3): 441–57.
19. Searle AG. Hereditary absence of spleen in the mouse. Nature. 1959; 184: 1419–20.
20. Searle AG. The genetics and morphology of two 'luxoid' mutants in the house mouse. Genet Res(Camb) 1964; 5: 171–97.
21. Wallace ME. Hydronephrosis in the mouse: the effects of the short-ear gene, sex and ureteral vascular system. Am J Anat 1976; 147: 19–32.
22. Held T, Paprotta I, Khulan J, Hemmerlein B, Binder L, Wolf S, et al. Hspa41-deficient mice display increased incidence of male infertility and hydronephrosis development. Mol Cell Biol. 2006; 26(21): 8099–108.
23. Lee J, Kim HJ, Moon JA, Sung YH, Baek I-J, Roh J, et al. Transgenic over expression of p23 induces spontaneous hydronephrosis in mice. Int J Exp Pathol. 2011; 92: 251–9.
24. Sällström J, Peuckert C, Gao X, Larsson E, Nilsson A, Jensen BL, et al. Impaired EphA4 signaling leads to congenital hydronephrosis, renal injury, and hypertension. Am J Physiol Renal Physiol. 2013; 305: F71–9.
25. Fenton RA, Knepper MA. Mouse models and the urinary concentrating mechanism in the new millennium. Physiol Rev. 2007; 87(4): 1083–112.
26. Couture-Haws L, Harris MW, Lockhart AC, Birnbaum LS. Evaluation of the persistence of hydronephrosis induced in mice following in utero and/or lactational exposure to 2, 3, 7, 8-Tetrachlorodibenzo-p-dioxin. Toxicol Appl Pharmacol. 1991; 107: 402–12.
27. Gakhar G, Wight-Carter M, Andrews G, Olson S, Nguyen TA. Hydronephrosis and urine retention in estrogen-implanted athymic nude mice. Vet Pathol. 2009; 46: 505–8.
28. Gamé X, Allard J, Escourrou G, Gourdy P, Tack I, Rischmann P, et al. Estradiol increases urethral tone through the local inhibition of neuronal nitric oxide synthase expression. Am J Physiol Regul Integr Comp Physiol. 2008; 294: R851–7.
29. Levin-Allerhand JA, Sokol K, Smith JD. Safe and effective method for chronic 17β-estradiol administration to mice. Contemp Top Lab Anim. 2003; 42(6): 33–5.
30. Okazaki T, Otaka Y, Wang J, Hiai H, Takai T, Ravetch JV, et al. Hydronephrosis associated with antiurothelial and antinuclear autoantibodies in BALB/c-*Fcgr2b*$^{-/-}$*Pdcd1*$^{-/-}$ mice. J Exp Med. 2005; 202(12): 1643–8.
31. Institute for Laboratory Animal Research. Guide for the care and use of laboratory animals. Washington, DC: National Academies Press; 2011.
32. Craig WD, Wagner BJ, Travis MD. Pyelonephritis: radiologic-pathologic review. RadioGraphics. 2008; 28: 255–76.
33. Franks LM. Normal and pathological anatomy and histology of the genital tract of rats and mice. In: Cotchin E, Roe FJC, editor. Pathology of laboratory rats and mice. Oxford: Blackwell Scientific; 1967, p. 469–499.
34. Cochlin DL, Dubbins PA, Goldberg BB, Alexander AA. Urogenital ultrasound. A text atlas. Philadelphia: J. B. Lippincot; 1994. p. 96.
35. Green RW. Kidneys. In: Green RW editor. Small animal ultrasound. New York: Lippincott-Raven; 1996, p. 197–210.
36. Thurston W, Wilson SR. The urinary tract. In: Rumack CM, Wilson SR, Charboneau JW, editor. Diagnostic ultrasound: volume 1. 3rd ed. St. Louis: Elsevier Mosby; 2005, p. 321–393.
37. Gaillard ET. Ureter, urinary bladder, and urethra. In: Maronpot RR, Boorman GA, Gaul BW, editor. Pathology of the mouse. Vienna, IL: Cache River Press; 1999, p. 235–258.
38. Cruz-Arámbulo R, Wrigley R, Powers B. Sonographic features of histiocytic neoplasms in the canine abdomen. Vet Radiol Ultrasound. 2004; 45(6): 554–8.
39. Homco LD. Lymph nodes. In: Green RW, editor. Small animal ultrasound. New York: Lippincott-Raven; 1996, p. 305–322.
40. Sokoloff L, Barile MF. Obstructive genitourinary disease in male STR/1N mice. Am J Pathol. 1962; 41(2): 233–46.
41. Eckhaus MA, Kopp JB. Renal diseases in genetically engineered mice. In: Ward JM, Mahler JF, Maronpot RR, Sundberg JP, Frederickson RM, editor. Pathology of genetically engineered mice. Ames, Iowa: Iowa State University Press; 2000, p. 347–364.
42. Sellars MEK. Ultrasound of the pediatric urogenital tract. In: Baxter BM, Sidhu PS, editor. Ultrasound of the urogenital system. New York: Thieme; 2006, p. 207–229.
43. Brant WE. The core curriculum. Ultrasound. Philadelphia: Lippincott Williams & Wilkins; 2001. p. 182.
44. Jiang Z, Asplin JR, Evan AP, Rajendran VM, Velazquez H, Nottoli TP, et al. Calcium oxalate urolithiasis in mice lacking anion transporter Slc26a6. Nat Genet. 2006; 38(4): 474–8.

Citation: Pathobiology of Aging & Age-related Diseases 2014, **4**: 24932 - http://dx.doi.org/10.3402/pba.v4.24932